AN EXPERIMENTAL SATELLITE-BASED FLOOD MONITORING SYSTEM FOR SOUTHERN QUEENSLAND, AUSTRALIA

B. Gouweleeuw[a]*, C. Ticehurst [a], P. Dyce[a] , J.P. Guerschman[a], A.I.J.M. Van Dijk[a], P. Thew [b]

[a]CSIRO Land and Water, Canberra, Australia –
(ben.gouweleeuw, catherine.ticehurst, peter.dyce, albert.vandijk)@csiro.au
[b]CSIRO Information, Communication and Technology Centre, Canberra, Australia – peter.thew@csiro.au

Abstract – A near real-time system is described, which provides spatial information of inland flood extent, using MOderate resolution Imaging Spectrometer (MODIS) optical reflectance and Advanced Microwave Scanning Radiometer (AMSR-E) microwave brightness temperature imagery, and flood volume through combination with a Digital Elevation Model (DEM). This information is an independent and useful addition to point data of gauged river flow at the in- and outlet of floodplains, typically only available with some latency, if at all. Comparison of satellite-derived volume estimates with those estimated from flow gauges for flood events on the lower-Balonne floodplain, South- Queensland, indicates flood volumes generally compare quite well at the onset of the flood events, but start to deviate at the peak flow into the flood recession. This is possibly explained by a combination of ungauged outflows, soil infiltration, evaporation and diversion of flood water into many large open reservoirs for crop irrigation.

Keywords: near real-time monitoring, satellite imagery, DEM, flood extent, flood volume

1. INTRODUCTION

The integration of remote sensing observations with stage data and flood modelling has the potential to provide improved support to a number of disciplines, such as water resources management and notably, flood forecasting. The ability of remote sensing technology to monitor the dynamics of hydrological events lies in its capacity to map surface water. For flood monitoring, remote sensing imagery needs to be available sufficiently frequently to capture subsequent inundation stages.

The most routinely applied method to map flood extent from space uses satellite reflectance data in the visible and thermal bands, due to its ability to contrast land and water at a relatively high spatial scale (e.g. Brackenridge and Anderson, 2006; Marcus and Fonstad, 2008). Data in this wavelength, however, is unable to penetrate cloud, which puts limitations on its daily use. This has prompted the use of data of longer wavelength, such as microwave data, as these are virtually all-weather, able to penetrate cloud (Brakenridge *et al.*, 2007; Bartsch *et al.*, 2008; Ticehurst *et al.*, 2009a). Synthetic Aperture Radar sensors have proven useful in mapping floods (Alsdorf *et al.*, 2007), but they are not routinely available at regional scales. Passive microwave sensors, however, acquire data at a high temporal frequency (1-2 times daily) on a near-global scale.

This paper describes a novel technique to monitor flood extent. It combines optical data and passive microwave data to optimize day-to-day continuity on the basis of cloud cover (Ticehurst *et al.*, 2009). Optical data of the two MODerate resolution Imaging Spectroradiometer (MODIS) sensors on board NASA's AQUA and TERRA satellites are available at a relatively high spatial and temporal resolution (250m-1km, twice daily for most parts of the world). Observations by the Advanced Microwave Scanning Radiometer (AMSR) for the Earth Observing System (EOS) are available at the same temporal resolution, but at comparatively coarse spatial resolution (5-70km). The smaller footprints correspond to the higher frequency bands, which are affected by precipitating cloud.

Mapped flood extent is subsequently overlaid on a DEM to estimate water elevations at the land-water contact. This provides an indirect measure of water surface height (Matgen *et al*., 2007, Penton and Overton, 2007) and, combined with the inundated surface, water volume (Miller, 1986). The horizontal and vertical accuracy of the DEM can have a large impact on the results (Schumann *et al.*, 2009). Even so, LeFavour and Alsdorf (2005) used the Shuttle Radar Topography Mission (SRTM, Slater *et al.*, 2006) DEM to obtain water height and surface water slope for long river reaches, despite its relatively large pixel size (90 m globally). Here, in the absence of a higher resolution DEM, and because of its general availability, enabling Australia wide transferability, we also used the SRTM DEM.

The monitoring system has been demonstrated to produce daily flood extent and volume for the lower-Balonne floodplain in the Condamine-Balonne catchment, Southern Queensland, Australia (Fig. 1). The catchment is situated in the upper northern headwaters of the Murray-Darling basin and during infrequent flood events is a significant source of water (CSIRO, 2008). These flood events occur once every two years on average and also provide flows into a heavily regulated system of river extractions and off stream open water storages for irrigation on the floodplain. Accurate information in near real-time is needed to effectively monitor how much water is taken by whom, but river water accounting during these flood events is hampered when flow gauges are overrun and the area is inaccessible.

It is proposed the remote sensing approach outlined above, using multiple sources of satellite data in combination with a DEM, can provide the required information on how much water is when and where and in a timely manner. To test this proposition, two flood events coinciding with the satellite sensor lifetimes, one of moderate size (peak-discharge at inflow point of 65 GL/day, Jan/Feb 2004) and the other of record-breaking size (peak-discharge at inflow point of over 240 GL/day, March 2010), are evaluated. Major flooding occurred again in Dec/Jan 2010/2011 in Queensland, including the lower-Balonne floodplain, identified as the state's single biggest natural disaster.

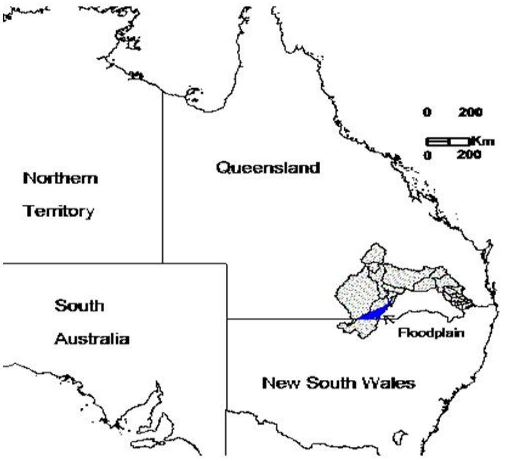

Fig. 1: Location of the Condamine-Balonne catchment (grey) and the lower-Balonne floodplain (blue).

2. METHODS

The satellite image processing steps are summarized only briefly here to facilitate a better understanding of the applied methods. A more detailed description for calculating flood extent is found in Ticehurst *et al.* (2009a).

2.1 MODIS processing

To map water in MODIS imagery the Open Water Index (OWI), following Guerschman *et al.* (2008), was used:

OWI = GVMI-EVI, if EVI <= 0.2 (1)
OWI = 0, if EVI > 0.2 (2)

, where Global Vegetation Moisture Index (GVMI) is calculated as (Ceccato *et al.*, 2002):

$$GVMI = \frac{(\rho_{NIR} + 0.1) - (\rho_{SWIR2} + 0.02)}{(\rho_{NIR} + 0.1) + (\rho_{SWIR2} + 0.02)} \quad (3)$$

and the Enhanced Vegetation Index (EVI), according to Huete *et al.*, 2002:

$$EVI = 2.5 \frac{\rho_{NIR} - \rho_{red}}{\rho_{NIR} + C_1 \cdot \rho_{red} - C_2 \cdot \rho_{blue} + L} \quad (4)$$

, where ρ_{NIR}, ρ_{RED}, ρ_{BLUE} and ρ_{SWIR2} are the reflectances in MODIS bands 1, 2, 3 and 6, respectively.

The OWI removes most of the vegetation water content on GVMI. A sigmoid function was used to convert OWI to Open Water Likelihood (OWL) as:

$$OWL = \frac{1}{1 + \exp(-50 \cdot (OWI - 0.1))} \quad (5)$$

This may be interpreted as the likelihood that a pixel represents open water, or alternatively, as the estimated fraction of water in the pixel (Guerschman *et al.*, 2008). A threshold of OWI≥ 0.2 was applied after Australian continent wide testing.

Daytime 500m reflectance MODIS imagery from Terra (MOD09A1) and Aqua (MYD09A1) was used, available for up to two times each day (depending on swath track). The accompanying MODIS quality band information was used to mask cloud pixels, and areas with EVI≥0.2 were also masked out. Estimation of the OWL for the remainder of the image produced values from 0 to 100 per cent. The two MODIS scenes for each day were combined, such that clouds and null pixels were replaced by the other scenes if it had real data. Where there was real data from both overpasses, the average value was used to reduce variation due to sun angle and noise.

Since the MODIS data provide the higher spatial resolution and OWL was shown to perform well for mapping water extent (Guerschman *et al.*, 2008), MODIS-OWL are given preference and AMSR-E is considered as a backup alternative in case of cloud cover.

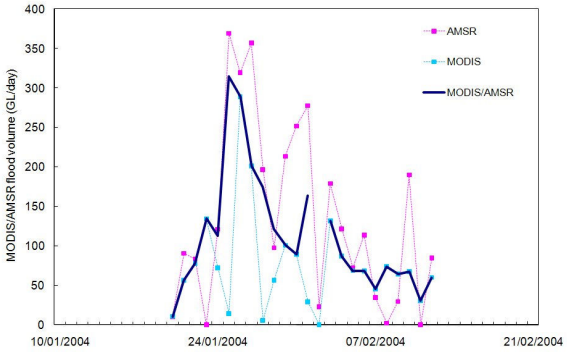

Fig. 2: Flood volumes derived from AMSR-E (pink), MODIS (light blue) and the combined MODIS/ AMSR-E (dark blue) imagery on the lower-Balonne floodplain for the Jan/Feb 2004 flood event. The relative weight of the two individual sensors in the combined MODIS/ AMSR-E curve depends on cloud cover fraction. The omitted data point in the MODIS/ AMSR-E curve represents Feb 2, when precipitation and cloud cover coincided and neither MODIS nor AMSR-E could be used.

2.2 AMSR-E processing

The AMSR-E sensor is flown on the same AQUA platform as MODIS. It tracks a descending and ascending orbit, sampling two images a day on average for most locations around the globe. The 37 GHz brightness temperature (T_b, K) is considered an appropriate compromise between spatial resolution and atmospheric interference effects to map surface water. It is used either at single (horizontal) polarization or as a Polarization Ratio (*PR*) to minimize atmospheric and soil temperature effects (Kerr and Njoku, 1993). Here, since 37 GHz data was sampled at day and night, the *PR* was used:

$$PR = (T_{bV} - T_{bH}) / (T_{bV} + T_{bH}) \quad (6)$$

, where T_{bV} and T_{bH} are vertically and horizontally polarized brightness temperatures, respectively.

Additionally, a rainfall mask, based on the difference between T_{bV} at 85 GHz and 22 GHz (Ferraro *et al.*, 1998), and a desert mask (Grody, 1991) to correct for vegetation effects, that complicate the separation between bare soil and water, are applied.

An open water extent map, based on MODIS-OWL, was used to relate the rainfall- and desert corrected PR (from here on referred to as CPR_{37}), to the proportion of water within a pixel. A single simultaneously acquired MODIS and AMSR-E image was used, coinciding with a large flood event, inundating several AMSR-E 37 GHz footprints completely. The resulting correlation is relatively low (R^2=0.42, RMSE=0.0056), possibly caused by MODIS/ AMSR-E sub-

pixel miss- registration. A lower threshold of 20% was applied, predominantly motivated by miss- classification of near-saturated soil, and other general data noise.

The relatively proportion of the small lower-Condamine floodplain size (3800 km^2) and the large AMSR-E 37 GHz footprint (14x8 km), prompted the downscaling of the AMSR-E derived open water fraction by means of the DEM. The DEM is derived from the 90m Shuttle Radar Topographic Mission (SRTM, Slater *et al.*, 2006), where aliasing was removed and gaps were filled (Gallant and Read, 2009). The AMRE-E footprint-average elevation was subtracted from the individual DEM pixels, thus eliminating large scale topography while conserving small-scale relief within the AMSR-E footprint. The fraction of water in the footprint was subsequently assigned to the equal lowest fraction in the processed DEM. This effectively translates into inundating the DEM within an AMSR-E footprint to achieve equvalent open water fractions. The result is a dynamic of water, flooding the depressions in the landscape on encounter. The disaggregated AMSR-E footprint was subsequently re-sampled to MODIS spatial resolution.

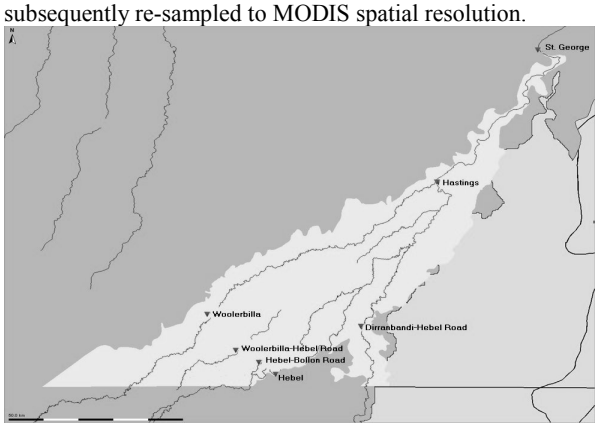

Fig. 3: Location of gauging stations on the lower-Balonne floodplain, north of the NSW/QLD border. St. George station is located upstream on the Balonne River and gauges inflow onto the floodplain. Downstream stations are Woolerbilla (Culgoa River), Woolerbilla-Hebel Road (Briarie Creek), Hebel-Bollon Road (Ballandool River), Hebel (Bokhara River) and Dirranbandi-Hebel Road (Narran River), which gauge the outflow from the floodplain

2.3 Water Volume processing

The water extent image is combined with the SRTM DEM, produced by Gallant and Read (2009), to calculate an estimate of the water volume on the floodplain. This can prove challenging, as the floodplain is extremely flat. Any noise in the MODIS/AMSR-E flood extent or the DEM affects the volume estimates.

Firstly, a water height surface is calculated for all pixels containing water (considered to be any pixels with >10% water to reduce confusion with near-saturated soil). To generate a water height surface, the DEM is registered with the flood extent image. Since a MODIS/AMSR-E pixel represents multiple DEM pixels, the DEM is used to calculate a water surface height for each flooded MODIS/AMSR-E pixel at the interface of each water surface feature. This is done by allocating the fraction of water in the MODIS /AMSR-E water pixel to the equal lowest fraction in the DEM. The highest flooded DEM value in the pixel is the assigned water surface height for that pixel.

The water heights at the corner points of an inundated surface are used to create triangles, which are subsequently interpolated to generate a water height surface. The water depth of each inundated pixel is subsequently derived by subtracting the DEM from the water height. Remnant noise fluctuations in the DEM and mismatches between the DEM and MODIS/AMSR-E images (caused by the flatness of the floodplain), do result in a number of negative water depth values within inundated surfaces. Finally, the water volume of all inundated pixels is obtained (multiplying water depth and pixel size) and summed to give the (daily) total water volume on the floodplain.

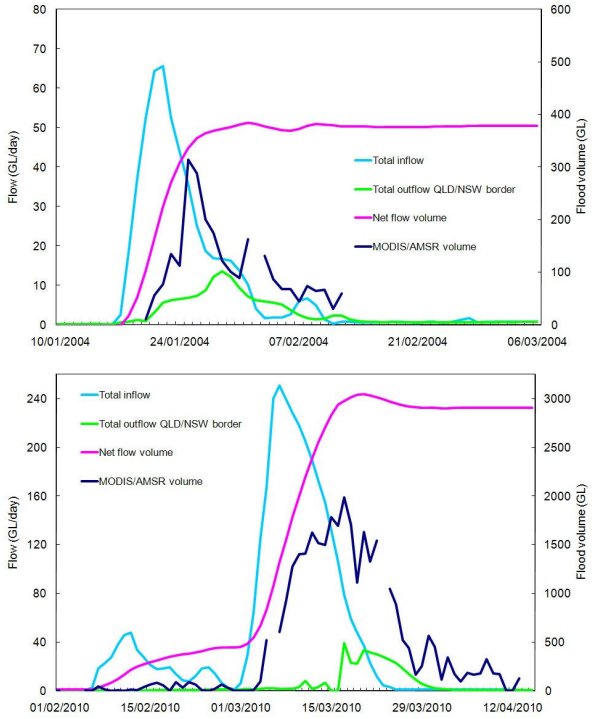

Fig. 4: Flood volume on the lower-Balonne floodplain for the flood event of Jan/Feb 2004 (upper panel) and March 2010 (lower panel) as estimated from MODIS/AMSR-E imagery and estimated from recorded flow. Note the different vertical scales.

3. RESULTS

Results with regard to the comparison of flood extent are described in Ticehurst *et al.* (2009a) and Ticehurst *et al.* (2009b). The results described here focus on the flood volume estimation and its comparison with on-ground station measurements of river flow.

3. 1 The January/February 2004 flood

Fig. 2 shows flood volumes estimated from MODIS reflectance data, AMSR-E brightness temperature data and the satellite data combined on the lower-Balonne floodplain for the Jan/Feb 2004 flood event. The AMSR-E flood volume estimate generally exceeds the MODIS estimate, probably due to its lower resolution and, therefore lower accuracy. As MODIS data is not available under cloud cover, AMSR-E data is used in that case instead. In turn, precipitating cloud conditions obstruct the reception of AMSR-E brightness temperature from the Earth's surface. During the flood peak, when cloud conditions occur, AMSR-E provides the more dependable flood volume estimate. The combination of MODIS and AMSR-E imagery results in a relatively

consistent curve with less day-to-day variation than the individual products. On Feb 2 precipitation and cloud cover coincided and neither MODIS nor AMSR-E could be used. This day is omitted from further analysis.

Fig. 4 (upper panel) shows the total inflow onto the lower-Balonne floodplain for the Jan/Feb 2004 flood event, as gauged by St. George station and the total outflow from the Queensland (QLD) part of the flood plain, as gauged by five stations just north of the New South Wales (NSW) border (Fig. 3). At the onset and peak of the flood event, the timing and total water volume on the floodplain estimated from the MODIS/AMSR-E images (just over 300 GL on Jan 25) agree quite well with the net volume assessed from recorded flow, albeit with a 1-2 day delay, possibly caused by initial water losses through soil infiltration, river water diversions or a delayed reaction of flow in the channels to the incoming river water. In the flood recession, however, the satellite-derived volume rapidly declines to about 60 GL, while water volume from flow records further increases to subsequently level out at 380 GL.

3. 2 The March 2010 flood

Fig. 4 (lower panel) shows the combined MODIS/AMSR-E estimation of flood volume for the March 2010 event (note the very different vertical scale). Estimates are not available for March 6, just after the onset of the flood and March 23, towards the recession of the flood. On both days almost complete cloud-cover coincides with incomplete AMSR-E footprint coverage.

In terms of magnitude, the March 2010 flood is nearly 10-fold the size of the Jan/Feb 2004 event. The pattern, however, is comparable. While satellite-derived flood volume shows a (slightly delayed) steep rise, peaks and declines (to about 150 GL), volumes estimated from flow gauges show a steep(er) increase to peak at 3000 GL to decline slightly and level out at 2850 GL. It should be noted that the flow gauge data provided by the Queensland Department of Environment and Resource Management (QDERM) are preliminary figures. Due to adjustments to the respective rating curves, the official figures, once released, are expected to be higher (QDERM, pers. comm.).

DISCUSSION

4. 1 Satellite-derived vs. flow gauged water volume

The observed difference between satellited-derived flood volume and volume derived from flow gauges can be explained by a number of processes.

1. Losses to evaporation and infiltration

Fig. 5 shows the development of the MODIS/AMSR-E open water extent for the 2004 flood on the lower-Balonne flood-plain. Assuming the difference in flow volume (315 GL) either infiltrates or evaporates over the maximum flooded area of just over 40.000 ha, this would amount to an 800 mm depth of water, almost twice the long-term average yearly rainfall of about 450mm. While it is improbable the total volume of water could be absorbed by infiltration, initial losses are reported to be potentially large. The cultivated part of the floodplain is covered by a Vertosol. This black soil

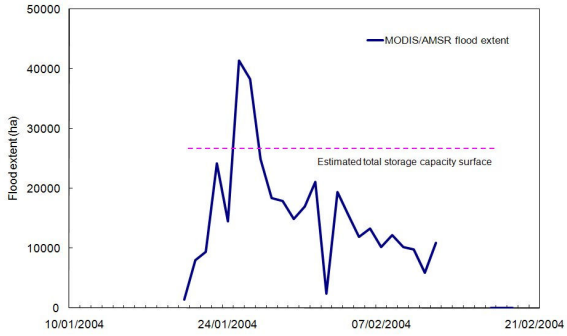

Fig. 5: MODIS/AMSR-E derived flood extent on the lower-Balonne floodplain for the Jan/Feb 2004 flood event. Also indicated is the estimated total storage capacity surface (Apan and Sternes, 2006).

type cracks under drying conditions and swells under wetting conditions, resealing the cracks in the process. At maximum development, the cracks measure typically 2-3 cm in width at the soil surface and 60-90 cm in depth (Smith, 2008). Reported infiltration losses are extremely variable, under varying experimental ponding conditions, ranging between 0.1-4 ML/ha (Chapman, 1982), 7-14 Ml/ha (Bridge and Muchow, 1982) and 1.8 Ml/ha (Muchow and Wood, 1981). This would translate into a total of anywhere between 4-560 GL for the 2004 flood event (40.000 ha maximum flood extent) and 24-3360 GL for 2010 (240.000 ha maximum flood extent). This could potentially explain all, or at least a significant part, of the 315 GL (2004) and 2700 (2010) flood volume difference, respectively. Initial losses for these flood events, however, are estimated to be relatively small due to rainfall on the floodplain prior to the flood, which wetted up the soil (QDERM, 2004) and as indicated by the smaller flood prior to the March 2010 flood. Data from Donohue *et al.* (2010) suggests Penman potential evaporation was between 8-10 mm/day on the lower-Balonne floodplain between 20 Jan–13 Feb 2004, resulting in an estimated 30-35 GL evaporative loss from open water, and a 10-fold of that for the March 2010 flood event (mainly due to the much larger flooded surface).

1. Water leaves the floodplain ungauged

The relatively low recorded outflow at the southern edge of the floodplain might be explained by water leaving the Queensland part of the floodplain ungauged. The lower-Balonne floodplain south of the Hastings bifurcation is a gently sloping, flat area (Fig. 3). River streams and creeks are shallow and easily overflow in a flood situation, generating an inland delta of flood ways over the floodplain. This is evident from Fig. 6, which shows a succession of satellite-derived flood extents. The four images are taken from the experimental Condamine-Balonne system. While these shallow streams by-pass the gauges in the larger rivers and creeks, water harvested from these shallow streams on the floodplain is not allocated or metered, and hence largely unaccounted for. The imagery for the March 2010 flood event shows substantial outbreaks of flood water by-passing flow gauges towards the south of the lower-Balonne floodplain and towards the south-east, both over the NSW/QLD border.

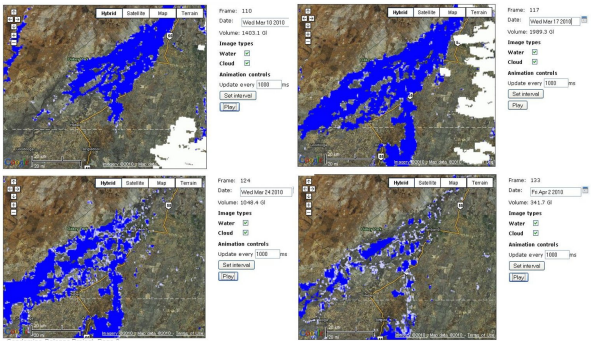

Fig. 6: A succession of 4 satellite-derived flood extent maps from march 2010, grabbed from the experimental real-time Condamine-Balonne monitoring system. The imagery clearly shows outbreak of flood water by-passing flow gauges, towards the south of the lower-Balonne floodplain and the south-east, both over the NSW/Queensland border.

2. Diverted river water and/or harvested floodplain water collected in storage

In 2004, the total capacity of open storage structures was an estimated 1200 GL (about three times the net flow volume recorded for the Jan/Feb 2004 flood event) with a total surface of 26,700 ha (Apan and Sternes, 2006). This combines to an average storage depth of about 4.5m. Fig. 7 illustrates a flooding scenario, showing a succession of three NW-SE cross-sections over the lower-Balonne floodplain. Due to the steep gradient of the constructed dam walls, open water extent in the storages remains unchanged over the course of a flood event, as water volume increases. In a flood recession, water extent in the rivers decreases (Fig. 7c). As the MODIS/AMSR-E algorithm relates flood volume to flood extent, it computes an overall decrease in volume, not registering the increase in storage volume.

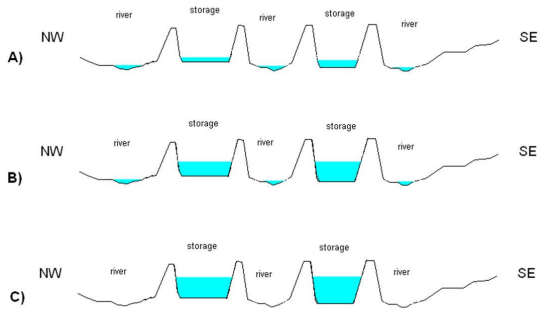

Fig. 7: A flooding scenario, as illustrated by a succession of three NW-SE cross-sections (A-C) over the lower-Balonne floodplain. While storages fill up, water extent remains unchanged.

A summary report of flows in Queensland for the lower-Balonne Jan/Feb 2004 flood event (QDERM, 2004) estimates a total volume of water diversion/extractions of 295 GL between the inflow at St. George station and the five outflow gauges (Fig.3). If it is assumed the diverted/extracted water is put in open water storage, open water extent is not increased, due to the steep-walled ring-tanks, leaving the added water undetected. The total volume of diverted/ extracted water (295 GL) subtracted from the difference between satellite-derived and gauged volume (380 GL), leaves a total of 85 GL for losses. A summary of flows report for the March 2010 flood was not yet available at the time of writing.

4. 2 Future work

Water depth data in the storage basins would provide valuable data in addition to the satellite-based water volume estimation. This information could be provided by, e.g. telemetered gauges or satellite altimetry. Whereas the installation and metering of gauges may prove costly, satellite altimetry is attractive, as point observation data from the Environmental Satellite (EnviSat) Radio Detection And Ranging (RADAR) Altimeter-2 and Jason-1 satellite is operationally available. If aligned with the satellite altimeter track, a maximum temporal resolution of 10 days allows for the assessment of water heights in target storage tanks before, during and after a flood event.

Additional satellite imagery sources may provide data redundancy and increase system reliability and accuracy. Satellite-based RADAR instruments are able to monitor floods on 1 km resolution with a 2-3 day temporal resolution (EnviSat Advanced Synthetic Aperture Radiometer (ASAR) Global Mode (GM)), while even higher resolution (~75 m) is available in Imaging Mode (IM), albeit with a relatively low temporal resolution (up to 35 days).

5. CONCLUSIONS

While initial losses due to dry antecedent conditions may be significant in a flood situation, these losses are estimated to be limited for the two flood events under consideration, due to rainfall on the lower-Balonne floodplain prior to the onset of the flood. In a flood event, the overtopping of rivers, generating overland flow in shallow streams, is a predominantly natural process, possibly enhanced locally by man-made structures. Evidence is found in the succession of flood extent maps for the March 2010 flood event that substantial outbreaks of flood water by-passing flow gauges have occurred.

ACKNOWLEDGEMENTS

This work has been carried out as part of the Condamine-Balonne Project in the CSIRO Water for a Healthy Country Flagship, funded by the Australian National Water Commission under the Raising National Water Standards Program. The authors wish to thank QDERM for providing the river gauge data, the summary of flows report for the Jan/Feb 2004 flood event and valuable insights in the hydrological functioning of the lower-Balonne floodplain.

REFERENCES

Alsdorf, D. E., P. Bates, J. Melack, M. Wilson, and T. Dunne (2007b), Spatial and temporal complexity of the Amazon flood measured from space, *Geophys. Res. Lett.*, *34*, L08402, doi:10.1029/2007GL029447.

Apan, A. and P. Sternes (2006), Mapping and spatio-temporal analysis of flooded and inundated areas in the Lower Balonne Floodplain, Queensland, Australia. *WSEAS Transactions on Environment and Development*, 4(2), 360-367.

Bartsch, A., M. Doubkova, C. Path, D. Sabel, W. Wagner and P. Wolski (2008), River flow and wetland monitoring with ENVISAT ASAR global mode in the Okavango Basin and Delta. *Proceedings of the Second IASTED Africa WRM Conference*, September 8-10, 2008, Gaborone, Botswana.

Brakenridge, R. and E. Anderson (2006), MODIS-based flood detection, mapping and measurement: The potential for operational hydrological Applications. J. Marsalek et al. (Eds.) Transboundary Floods: Reducing the Risks through Flood Management, 72, 1-12.

Brakenridge, G.R., S.V. Nghiem, E. Anderson and R. Mic (2007), Orbital microwave measurement of river discharge and ice status. *WRR.*, 43, W04405, 16pp.

Bridge, B.J. and R.C. Muchow (1982), Soil water relationships for Cununurra Clay and Ord Sandy Loam in the Ord River Irrigation Area. Tropical Agronomy Technical Memorandum No. 30, CSIRO Div. of Trop. Crops and Pastures, CISRO, Canberra, Australia

Ceccato, P, N. Gobron, S. Flasse, B. Pinty and S. Tarantola (2002), Designing a spectral index to estimate vegetation water content from remote sensing data: Part 1 Theoretical Approach. *Remote Sensing of Environment*, 82,188-197.

Chapman, A.L. (1982), Evidence of high water infiltration rates in a rice field on Cununurra clay, Ord Irrigation Area, W.A. Tropical Agronomy Technical Memorandum No. 32, CSIRO Div. of Trop. Crops and Pastures, CSIRO, Canberra.

CSIRO (2008), Water Availability in the Condamine-Balonne, A report to the Australian Government from the CSIRO Murray-Darling Sust. Yields Pr. CSIRO Tech. Rep.

Donohue, R.J., T.R. McVicar and M.L. Roderick (2010), Assessing the ability of potential evaporation formulations to capture the dynamics in evaporative demand within changing climate. *Journal of Hydrology,* 386, 1-4, 186-197, doi:10.1016/j.jhydrol.2010.03.020

Ferraro, R.R., E.A. Smith, W. Berg and G.J. Huffman (1998), A screening methodology for passive microwave precipitation retrieval algorithms. *J. Atm. Sc.*, 55, 1583-1600.

Gallant, J.C. and A. Read, A. (2009), Enhancing the SRTM data for Australia, *Geomorphometry 2009*, Ed. R.Purves, S.Gruber, R.Straumann & T.Hengl. University of Zurich, Zurich, 2009.

Grody, N.C. (1991), Classification of snow cover and precipitation using the Special Sensor Microwave/Imager (SMM/I). *Journal of Geophysical Research*, 96, 7423-7435.

Guerschman, J.P., A.I.J.M. Van Dijk, T.R. McVicar, T.G. Van Niel, L. Lingtao, Y. Lui and J. Peña-Arancibia (2008), Actual evapotranspiration and water balance estimates from satellite observations over the Murray-Darling Basin. Canberra, *CSIRO Science Report*.

Huete, A., K. Didan, T. Muira, E.P. Rodriguez, X. Gao and L.G. Ferreira (2002), Overview of the radiometric and biophysical performance of the MODIS vegetation indices. *Remote Sensing of Environment*, 83, 195-213.

Kerr, Y.H. and E.G. Njoku (1993), On the use of passive microwaves at 37 GHz in remote sensing of vegetation. *Int. J. of Rem. Sens.*, 14(10), 1931-1943

Marcus, W.A. and M.A. Fonstad (2008), Optical remote mapping of rivers at sub-meter resolutions and watershed extents, *Earth Surf. Processes Landforms*, 33, 4-24.

LeFavour, G. and D. Alsdorf (2005), Water slope and discharge in the Amazon River estimated using the shuttle radar topography mission digital elevation model. Geophysical Research Letters, 32, L17404

Matgen , P., G. Schumann, J. Henry, L. Hoffmann and L. Pfister (2007), Integration of SAR-derived inundation areas, high precision topographic data and a river flow model toward real-time flood management. International Journal of Applied Earth Observation Geoinf., 9(3), 247-263.

Miller, S.T. (1986), The quantification of floodplain inundation by the use of Landsat and metric camera information, Belize, Central America. Proceedings, 7th Int. Symp., ISPRS, Comm. VII, Enschede August 1986, 733-738.

Muchow, R.C. and Wood, I.M. (1981), Pattern of infiltration with furrow irrigation and evapotranspiration of kenaf (Hibiscus cannabinus) grown on Cununurra clay in the Ord Irrigation Area. Austr. J Exp Agric Anim Husb 21:101–108.

Njoku, E.G. (1999), *AMSR Land Surface parameters. Algorithm Theoretical Basis Document, Version 3.0*. Pasadena, CA, USA, NASA JPL.

Overton, I.C., K. McEwan, C.Gabrovsek, and J.R Sherrah (2006), The River Murray Floodplain Inundation Model (RiM-FIM), Hume Dam to Wellington, CSIRO WfHC Tech. Rep.

Penton, D.J., and I.C. Overton (2007), Spatial modelling of floodplain inundation combining satellite imagery and elevation models. In Oxley, L. and Kulasiri, D. (Eds) Proc. of MODSIM 2007, Dec 2007.

QDERM (2004), The Lower Balonne January/February 2004 Flow Event- Summary Report of flows in Queensland, DERM Internal Report, St George office.

Schumann, G., P.D. Bates, M.S. Horritt, P. Matgen and F. Pappenberger (2009), Progress in integration of remote-sensing derived flood extent and stage data and hydraulic models, *Reviews of Geophysics*, 47, RG40001, doi:10.1029/2008RG000274.

Slater, J.A., G. Garvey, C. Johnston, J. Haase, B. Heady, G. Kroenung, and J. Little (2006), The SRTM data "finishing" process and products. *Photogr. Eng. & RS*, 72 (3), 237-247.

Smith, L.C. (1997), Satellite remote sensing of river inundation area, stage, and discharge: A review. *Hydrological Processes*, 11, 1427-1439.

Ticehurst, C. J, P. Dyce and J.P. Guerschman (2009), Using passive microwave and optical remote sensing to monitor flood inundation in support of hydrologic modelling, *18th World IMACS/MODSIM Congress, Cairns, Australia*.

Ticehurst, C. J, A. Bartsch , M. Doubkova and A.I.J.M. Van Dijk (2009), Comparison of ENVISAT ASAR GM, AMSR-E Passive Microwave, and MODIS Optical Remote Sensing for Flood Monitoring in Australia, *Earth Obs. and Water Cycle Science, ESA SP-674, Frascati, Italy.*